First International Conference on Innovative Engineering Systems (ICIES): Local Conference

Evaluation of Strain Gauge Factors of Graphene Ribbon Models Based on First-Principles Electronic-State Calculations

Mohammed Gamil[1,*], Koichi Nakamura[1,2], Ahmed M.R. Fath El-Bab[3], Osamu Tabata[4], Mohamed Serry[5], Ahmed Abd El-Moneim[1]

[1]Material Science and Engineering Department, Egypt-Japan University of Science and Technology (E-JUST), Alexandria, Egypt, gameel1353@yahoo.com

[2]Center for the Promotion of Interdisciplinary Education and Research, Kyoto University, Kyoto, Japan

[3]Mechanical Engineering Department, Faculty of Engineering, Assiut University, Assiut, Egypt

[4]Department of Micro-Engineering, Kyoto University, Kyoto, Japan

[5]Mechanical Engineering Department, American University in Cairo (AUC), Cairo, Egypt

***Abstract*— The present work has simulated the piezoresistivity coefficient in graphene ribbon based on the first-principles electronic-state calculation method. The carrier conductivity along the graphene ribbon models have been calculated using band carrier densities and their corresponding effective masses derived from the one-dimensional band diagram. The longitudinal and transverse gauge factors are large in our calculation, and the zigzag graphene ribbon is a high potential material with high piezoresistivity.**

Keywords-Graphene ribbon; low-dimensional semiconductor; giant piezoresitivity; micro-electro-mechanical systems (MEMS); first-principles calculation

I. INTRODUCTION

Graphene sheet-one-atom-thick two-dimensional (2D) layers of sp^2-bonded carbon (C) that illustrated in Fig. 1 is the thinnest known material which gathered a lot of attention after its discovery by Novoselov et al. because of unique electrical and mechanical properties such as high electron mobility and stiffness [1,2]. The piezoresistance effect (gauge factor) defines the electrical resistivity change of semiconductors under mechanical stress [3]. With the ardent interest to merge graphene into piezoresistor applications, researchers are driven to study the piezoresistance effect of graphene sheets made via different methods. Lee et al. reported in their study that the gauge factor of graphene grown on Ni and Cu films by chemical vapor deposition was 6.1, with an applied strain of up to 1% [4]. Chen et al. found that the gauge factor of mechanically exfoliated graphene is nearly 150 [5]. Hosseinzadegan et al. reported in their work that the gauge factor of graphene prepared by chemical vapor deposition on Si/SiO_2 wafer is 18,000 [6]. A recent theoretical work predicts the splitting of the graphene band-gap from conductive to semiconducting state upon applied strain [7]. However, many others have claimed that single-layer graphene cannot have a band-gap [8]. If a band-gap exists, the strain-induced band-gap modulation could be one source of piezoresistivity in graphene [6].

In this work, first-principles band calculation technique based on density functional theory was used to evaluate the gauge factors of graphene models, the gauge factor will be evaluated by calculation of the first-principles band structure [9,10], determination of the band carrier densities and determination of the band effective masses for both strain-free and strain models.

II. METHOD OF CALCULATION

First-principles calculations of the periodic boundary models for graphene have been carried out by FHI98MD [11] program package based on the density functional theory (DFT) [12]. For the DFT exchange-correlation interaction, the generalized-gradient approximation (GGA) method was used [13]. We adopted the three dimensional supercell approximation technique with norm-conserving pseudo potentials prepared according to the Hamann method [14] and wave functions with plane-wave expansion.

First, zigzag and armchair models have been defined as shown in Fig. 2, where these models have been devised by cutting out a fragment with a one dimensional periodic boundary, and all dangling bonds of carbon atoms were terminated with hydrogen (H) atoms. The direction of the fragment which is parallel to the y direction can be defined as the longitudinal direction, while the parallel to the x direction can be considered as the transverse direction as illustrated in Fig. 2 (c). To represent graphene ribbons, the vacuum space about 5 Å along X direction is considered.

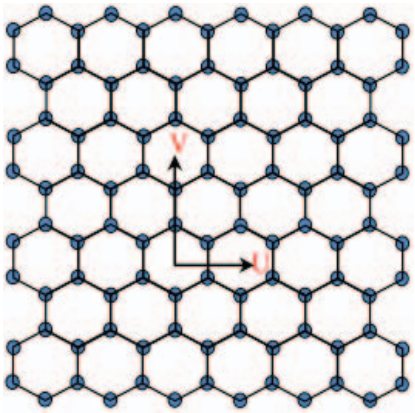

Figure 1 . Graphene Sheet.

978-1-4673-4439-5/12/$31.00 ©2012 IEEE

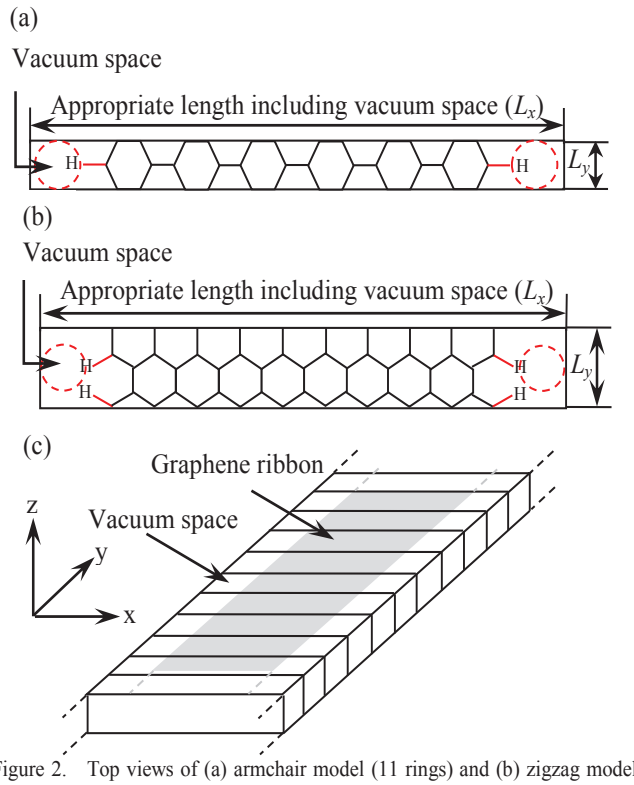

Figure 2. Top views of (a) armchair model (11 rings) and (b) zigzag model (17 rings), and (c) 3D-dimensional periodic boundary condition for these models.

III. Results and Discussion

A. Optimization of C-C length of graphene sheet.

C-C length of the graphene sheet in the strain free condition has been optimized. We find that the optimized value of the C-C length (Req) of graphene is 1.422 Å which is corresponding to the minimum total energy as illustrated in Fig. 3. Moreover, this value is corresponding to the obtained (1.42 Å) by Heyrovska [15].

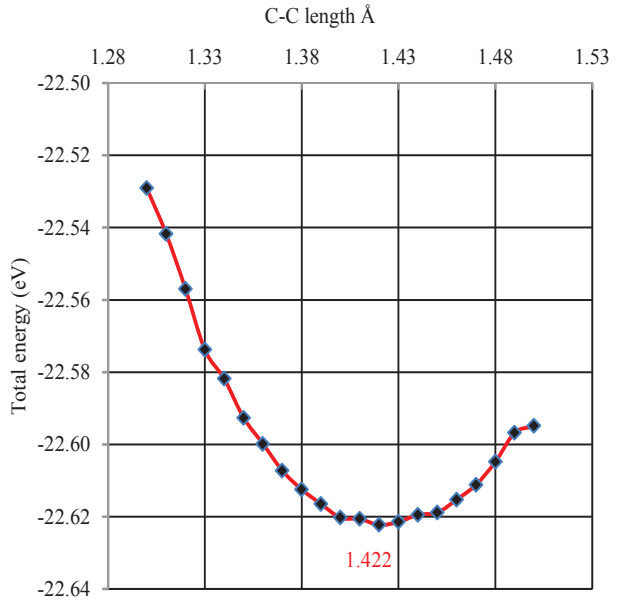

Figure 3. Total energy of graphene with respect to C-C length.

B. Partial optimization of strain condition for Poisson's ratios.

Optimization of strain condition for Poisson's ratio plays an important role for calculating the C-C length after applying longitudinal or transverse strain as indicated in equations (1).

$$\upsilon = -\frac{\varepsilon_{perp}}{\varepsilon_{axial}}, \quad (1)$$

where ε_{perp} is the transverse strain (perpendicular to the applied load) and ε_{axial} is the axial strain (in the direction of the applied load). Two different strain models were suggested, the first is the V strain model while the second is the U strain model as illustrated in Fig. 1. Both of them will be discussed in details as follows:

1) V strain model

The effect of uniaxial tensile strain on structure was represented by partial optimization with a fixed lattice constant along the tensile direction as illustrated in Fig. 4(a). For 1% uniaxial tensile strain in the V direction, we set V lattice constant at 1.43622 Å (=1.422×1.01) and optimized U lattice constant to 1.418 Å, Therefore the Poisson's ratio is determined as $\upsilon = 0.28$ [16-18].

2) U strain model

In this model 1% strain was applied in U direction (constant) while the strain in V direction is then optimized as illustrated in Fig. 4 (b). From the optimized value we can easily calculate the Poisson's ratio from the equation 1. $\upsilon = 0.14$ [19-21].

All the structural parameters of the graphene ribbon models such number of C atoms (N_C), number of H atoms (N_H), and the model dimensions are tabulated in Table I.

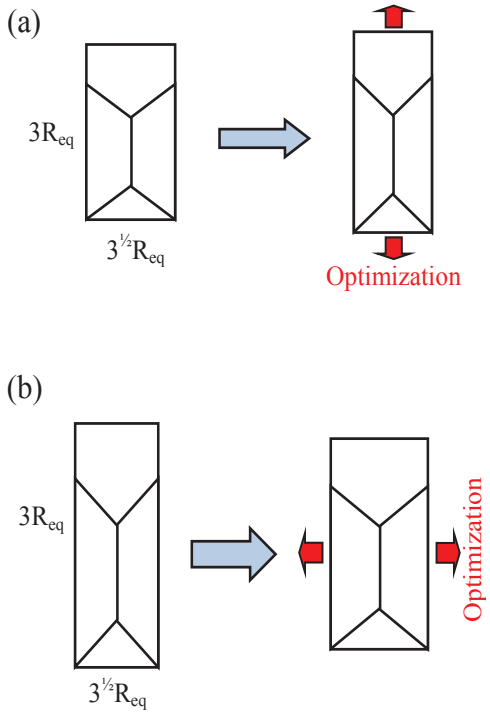

Figure 4. (a) V strain model, (b) U strain model.

TABLE I. STRUCTURAL PARAMETRES OF GRAPHENE MODELS

Model type		(N_C)	(N_H)	Model dimensions (A°)				
				L_x (Fixed)	L_y			L_z (Fixed)
					Strain free	Longitudinal strain	Transverse strain	
Armchair model	9 rings	20	2	27.108	2.463	2.488	2.460	10.000
Zigzag model	13 rings	54	4	38.924	4.266	4.309	4.260	

C. Modeling and calculation of armchair models

The whole image of band energy diagram of the 9-ring armchair model is shown in Fig. 5. The valence band (blue lines) maximizes and the conduction band (red lines) minimizes at the Y point, respectively, and accordingly, the intrinsic armchair graphene ribbon can be considered as a semi-metal or zero-band gap semiconductor. In detail, the highest subband of the valence band and the lowest subband of the conduction band are in double degeneracy at the Y point, in the vicinity of the Fermi energy. This feature can be also derived by the simple Hückel method qualitatively for the armchair models, and the π orbitals of 9-ring and 13 -ring armchair models for the degenerate subbands at the Y point closely resemble each other as shown in Fig. 6. As the common characteristic of the armchair models, the π orbitals of all of armchair models are localized at the edges of graphene ribbon, and no conductance path exists in the center of graphene ribbon. The interaction due to π orbitals along the longitudinal direction is very small because of the non-bonding state due to the antisymmetric relation for the translation with the phase factor $e^{i\pi y/L_y}$, and accordingly, the band energy variation of these degenerate subbands with respect to k point is quite small near the Y point. As a result, low conductivity with heavy effective mass can be explained by using the band orbital interaction.

Variations of the band structures with respect to the strain models have been observed. As it is clear from the band energy diagram shown in Fig. 7, the degenerate subbands in the vicinity of the Fermi energy are not lifted by the longitudinal or transverse strain effect, and the feature of conductivity based on the band energy diagram will not change so much. These features are in good agreement with quite small band orbital interaction as shown in Fig. 6.

D. Modeling and calculation of zigzag models

The whole image of band diagram of the 13-ring zigzag model is shown in Fig. 8. The valence band maximizes and the conduction band minimizes near the Γ point, respectively. Fig. 9 represents the strain-free and the strain models band energies diagrams for 13-ring zigzag models. As compared with the armchair models, the variation of band energy diagrams of the zigzag models by the strain is much more sensitive. In particular, the characteristics of valence-band top and conduction-bad bottom subbands near the Fermi energy are caused by both of the longitudinal and transverse strains. Actually, the π orbitals of valence-band top and conduction band-bottom are delocalized, and the band orbital interaction is easy to be caused due to strains.

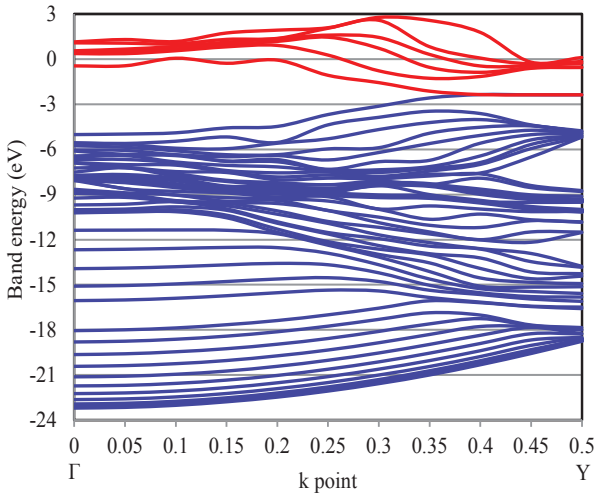

Figure 5. Band energy diagram of 9-ring armchair model.

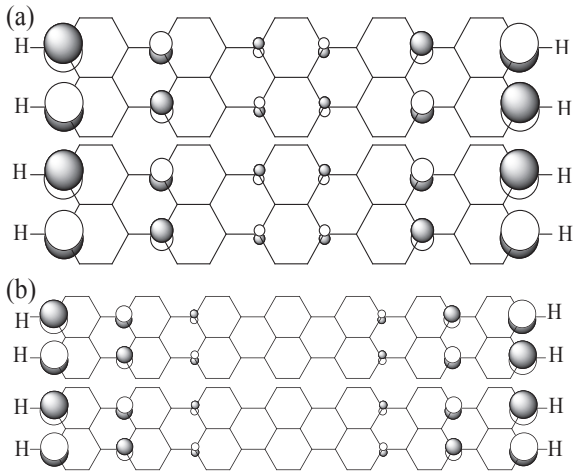

Figure 6. Degenerate π orbitals at Y point near the Fermi energy for the (a) 9-ring and (b) 13-ring armchair models with 2 unit cells.

E. Evaluation of strain gauge factors

1) Carrier conductivity

The electrical conductivity G or the electrical resistivity ρ can be represented in terms of carrier density and effective mass [22]. Variations of band structure will exert an influence on them, and frequently contribute to a sudden turn of the conductivity. In this paper, we have introduced the band carrier densities and their corresponding effective masses for each energy band, and the conductivity has been added up over all valence and conduction bands as follows,

$$G=\frac{1}{\rho}=e^2\sum_{j\epsilon Carrier}\frac{n_j\tau_{e,j}}{m^*_{e,j}}, \quad (2)$$

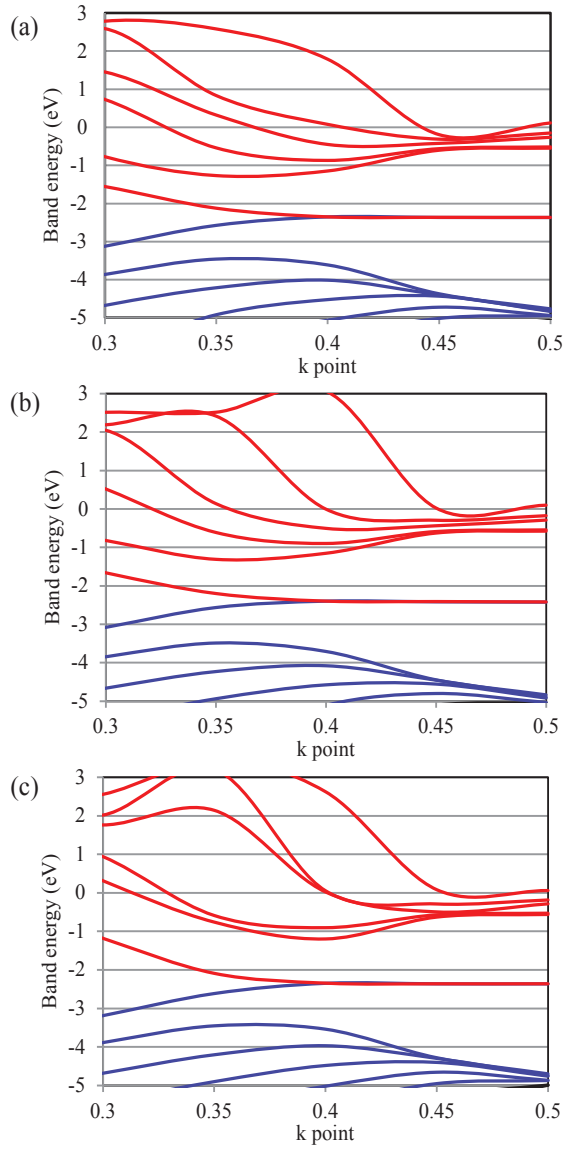

Figure 7. Band energy diagrams for 9-ring armchair (a) no strain model (b) longitudinal strain model (c) transverse strain model.

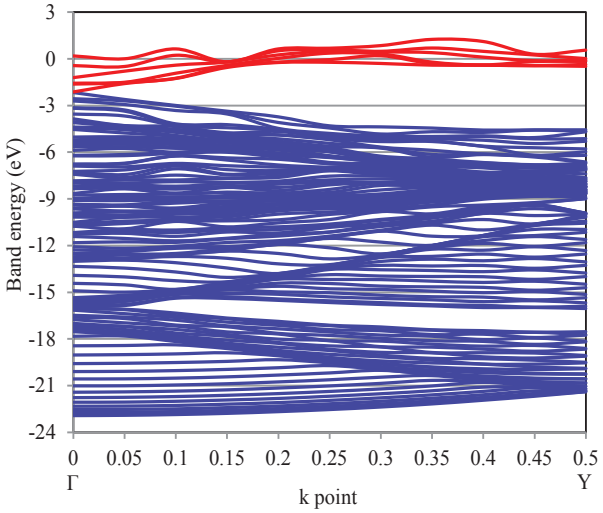

Figure 8. Band energy diagram of 13-ring zigzag model.

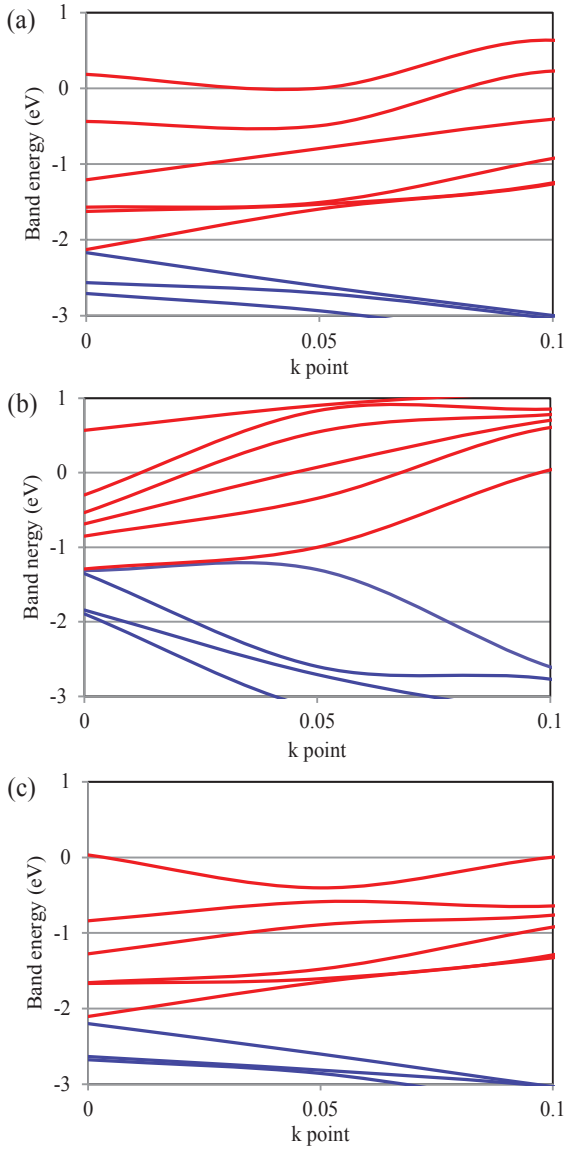

Figure 9. Band energy diagrams for 13-ring zigzag (a) no strain model (b) longitudinal strain model (c) transverse strain model.

Where n_j is the jth conduction band (CB) carrier electron area density, $m^*_{e,j}$ is the effective masse at the lowest conduction band, $\tau_{e,j}$ is the relaxation time, and e^2 is the square of the absolute value of the elementary electric charge. Subscript e denotes electron carriers. The band carrier densities are controlled by the Fermi energy E_F and temperature T,

$$N = 2 \sum_{j} \sum_{k_y} w_{k_y} \left[\exp\left(\frac{E_{j,k_y} - E_F}{K_B T} \right) + 1 \right]^{-1}, \quad (3)$$

$$n_j = \frac{2}{S} \sum_{k_y} w_{k_y} \left[\exp\left(\frac{E_{j,k_y} - E_F}{K_B T} \right) + 1 \right]^{-1}, \quad (4)$$

Where N is the total number of valence electrons in the model, E_{j,k_y} is the band energy of the jth band at the k_y point, w_{k_y} is the k-point weight for k_y, S is the surface area of the graphene model ($S = L_x \times L_y$), and K_B is the Boltzmann

constant. We have performed a sampling with 11 k_y points along the Γ–Y path. The values of Fermi energy (E_F), and n_j for each graphene model have been solved according to equations (3) and (4) respectively. The effective mass is generally a 3 × 3 tensor. The reciprocal matrix of effective mass is defined as [23].

$$\left(m^*\right)^{-1} = \frac{1}{\hbar^2}\begin{pmatrix} \frac{\partial^2 E}{\partial k_x^2} & \frac{\partial^2 E}{\partial k_x \partial k_y} & \frac{\partial^2 E}{\partial k_x \partial k_z} \\ \frac{\partial^2 E}{\partial k_y \partial k_x} & \frac{\partial^2 E}{\partial k_y^2} & \frac{\partial^2 E}{\partial k_y \partial k_z} \\ \frac{\partial^2 E}{\partial k_z \partial k_x} & \frac{\partial^2 E}{\partial k_z \partial k_y} & \frac{\partial^2 E}{\partial k_z^2} \end{pmatrix}, \quad (5)$$

where E is the band energy, and $\hbar$ is equal to Planck's constant divided by 2π. The band energies of our graphene models remain constant along the transverse directions, namely,

$$\frac{\partial E}{\partial k_x} = \frac{\partial E}{\partial k_z} = 0, \quad (6)$$

And therefore, the effective mass of the *j*th band for the graphene models can be defined simply as a scalar,

$$m_j^* = \hbar^2 \left(\frac{\partial^2 E_j}{\partial k_y^2}\right)^{-1}, \quad (7)$$

And the second derivative on the right hand of equation (7) has been estimated numerically as

$$\frac{\partial^2 E_j[k_y]}{\partial k_y^2} = \frac{E_j[k_y+\Delta k_y]+E_j[k_y-\Delta k_y]-2E_j[k_y]}{(\Delta k_y)^2}, \quad (8)$$

with $\Delta k_y = 0.05 \times (2\pi / L_y)$ For the relaxation time in graphene systems, we have introduced the approximation that all of the band relaxation times are equal and constant regardless of stress [9,10]. This procedure seems to be rough to some extent, but the variation rate of carrier conductivity can be easily and adequately represented in consideration of the canceling of almost part of band relaxation times.

2) Gauge factor

$$\text{G.F} = \frac{R_\alpha - R_0}{R_0} \Big/ \varepsilon_\alpha, \quad (9)$$

where R_α and R_0 are the graphene resistances at applied strain (ε_α), and at no strain respectively. From equations (2) and (9), the gauge factor equation can be written as follows:

$$\text{G.F} = \frac{1}{\varepsilon_\alpha}\left(\frac{\sum_{j \epsilon Carrier} \frac{n_{j,0}}{m^*_{e,j,0}}}{\sum_{j \epsilon Carrier} \frac{n_{j,\alpha}}{m^*_{e,j,\alpha}}} - 1\right), \quad (10)$$

Using the data obtained from the energy diagrams which are tabulated in table II, we can easily calculate the values of the gauge factor for both armchair model and zigzag model as illustrated in Table III.

TABLE II. ARMCHAIR AND ZIGZAG MODEL PROPERTIES

Model type		E_F *(eV)*	$\sum_{j \epsilon Carrier} n_j$	$m^{*\,-1}_{e,j}$
Armchair 9-rings	*No strain model*	*-2.359*	7.490×10^{17}	*0.0286*
	Longitudinal strain	*-2.408*	7.496×10^{17}	*0.0447*
	Transverse strain	*-2.356*	7.489×10^{17}	*0.0408*
Zigzag 13-rings	*No strain model*	*-2.149*	1.909×10^{16}	*8.6424*
	Longitudinal strain	*-1.158*	1.031×10^{17}	*2.4308*
	Transverse strain	*-2.152*	1.127×10^{16}	*6.1671*

TABLE III. GAUGE FACTORS OF GRAHENE MODELS

Model type		*Gauge factor (G.F)*	
		Longitudinal strain model	*Transverse strain model*
Armchair model	*9-rings*	*56*	*42.4*
Zigzag model	*13-rings*	*34.2*	*137.4*

It was found that the carrier electron area densities of armchair model do not change due to any strains and the effective masses are very large regardless of strains. From the view point of piezoresistivity, the longitudinal and transverse gauge factors seem to be large because the variation ratios of inverse effective masses due to strain become large by high sensitivity with small values. As compared with the armchair model, drastic changes in the carrier electron area densities and effective masses due to strain can be observed in the zigzag model.

CONCLUSSION

In this paper, the gauge factors in armchair and zigzag graphene ribbon models on the basis of first-principles calculations have been simulated. The carrier conductivity of graphene ribbon has been calculated using band carrier densities and their corresponding effective masses. And we found the different characteristics in conductivity between armchair and zigzag models. The longitudinal and transverse gauge factors are large in our calculation, and the zigzag graphene ribbon is a high potential material with high piezoresistivity if we find good systems and conditions for graphene ribbons fabrication.

ACKNOWLEDGMENT

The authors gratefully acknowledge the Missions Sector-Higher Education Ministry, Egypt for financial support through this work.

REFERENCES

[1] D. R. Cooper, B. D'Anjou, N. Ghattamaneni, B. Harack, M. Hilke, A. Horth, et al., "Experimental review of graphene," arXiv preprint arXiv:1110.6557, 2011.

[2] K. Novoselov, A. Geim, S. Morozov, D. Jiang, Y. Zhang, S. Dubonos, et al., "Electric field effect in atomically thin carbon films," Science, vol. 306, pp. 666-669, 2004.

[3] A. A. Barlian, W. T. Park, J. R. Mallon, A. J. Rastegar, and B. L. Pruitt, "Review: Semiconductor piezoresistance for microsystems," Proceedings of the IEEE, vol. 97, pp. 513-552, 2009.

[4] Y. Lee, S. Bae, H. Jang, S. Jang, S. E. Zhu, S. H. Sim, et al., "Wafer-scale synthesis and transfer of graphene films," Nano letters, vol. 10, pp. 490-493, 2010.

[5] X. Chen, X. Zheng, J. K. Kim, X. Li, and D. W. Lee, "Investigation of graphene piezoresistors for use as strain gauge sensors," Journal of Vacuum Science & Technology B: Microelectronics and Nanometer Structures, vol. 29, pp. 06FE01-06FE01-5, 2011.

[6] H. Hosseinzadegan, C. Todd, A. Lal, M. Pandey, M. Levendorf, and J. Park, "Graphene has ultra high piezoresistive gauge factor," 2012, pp. 611-614.

[7] Z. H. Ni, T. Yu, Y. H. Lu, Y. Y. Wang, Y. P. Feng, and Z. X. Shen, "Uniaxial strain on graphene: Raman spectroscopy study and band-gap opening," Acs Nano, vol. 2, pp. 2301-2305, 2008.

[8] A. H. C. Neto, F. Guinea, N. Peres, K. Novoselov, and A. Geim, "The electronic properties of graphene," Reviews of modern physics, vol. 81, p. 109, 2009.

[9] K. Nakamura, Y. Isono, and T. Toriyama, "First-Principles Study on Piezoresistance Effect in Silicon Nanowires," Jpn. J. Appl. Phys, vol. 47, No. 6, 2008, pp. 5132–5138.

[10] K. Nakamura, Y. Isono, T. Toriyama, and S. Sugiyama, "Simulation of piezoresistivity in n-type single-crystal silicon on the basis of the first-principles band structure," Physical Review B, vol. 80, p. 045205, 2009.

[11] M. Bockstedte, A. Kley, J. Neugebauer, and M. Scheffler, "Density-functional theory calculations for poly-atomic systems: electronic structure, static and elastic properties and ab initio molecular dynamics," Computer physics communications, vol. 107, pp. 187-222, 1997.

[12] P. Hohenberg and W. Kohn, "Inhomogeneous electron gas," Physical Review, vol. 136, p. B864, 1964.

[13] J. P. Perdew, K. Burke, and M. Ernzerhof, "Generalized gradient approximation made simple," Physical review letters, vol. 77, pp. 3865-3868, 1996.

[14] D. Hamann, "Generalized norm-conserving pseudopotentials," Physical Review B, vol. 40, p. 2980, 1989.

[15] R. Heyrovska, "Atomic structures of graphene, benzene and methane with bond lengths as sums of the single, double and resonance bond radii of carbon," arXiv preprint arXiv:0804.4086, 2008.

[16] J. P. Lu, "Elastic properties of carbon nanotubes and nanoropes," Physical Review Letters, vol. 79, pp. 1297-1300, 1997.

[17] M. Treacy, T. Ebbesen, and J. Gibson, "Exceptionally high Young's modulus observed for individual carbon nanotubes," Nature, vol. 381, pp. 678–680, 1996.

[18] A. Krishnan, E. Dujardin, T. Ebbesen, P. Yianilos, and M. Treacy, "Young's modulus of single-walled nanotubes," Physical Review B, vol. 58, p. 14013, 1998.

[19] D. Sánchez-Portal, E. Artacho, J. M. Soler, A. Rubio, and P. Ordejón, "Ab initio structural, elastic, and vibrational properties of carbon nanotubes," Physical Review B, vol. 59, p. 12678, 1999.

[20] K. Shintani and T. Narita, "Atomistic study of strain dependence of Poisson's ratio of single-walled carbon nanotubes," Surface science, vol. 532, pp. 862-868, 2003.

[21] T. Chang and H. Gao, "Size-dependent elastic properties of a single-walled carbon nanotube via a molecular mechanics model," Journal of the Mechanics and Physics of Solids, vol. 51, pp. 1059-1074, 2003.

[22] C. Kittel: Introduction to Solid State Physics (Wiley, New York, 2005), 8th ed., p. 200.

[23] J. M. Ziman: Principle of the Theory of Solids (Cambridge UniversityPress, New York, 1972) 2nd ed., pp. 183–186.